INTERNATIONAL JOURNAL FOR NUMERICAL METHODS IN FLUIDS
Int. J. Numer. Meth. Fluids 2009; **60**:809–825
Published online 10 September 2008 in Wiley InterScience (www.interscience.wiley.com). DOI: 10.1002/fld.1921

Boundary conditions at the interface between fluid layer and fibrous medium

H. X. Bai[1], P. Yu[1], S. H. Winoto[1] and H. T. Low[2,*,†,‡]

[1]*Department of Mechanical Engineering, National University of Singapore, 9 Engineering Drive 1, Singapore 117576, Singapore*
[2]*Division of Bioengineering Engineering, National University of Singapore, 9 Engineering Drive 1, Singapore 117576, Singapore*

SUMMARY

The flow through a channel partially filled with fibrous porous medium was analyzed to investigate the interfacial boundary conditions. The fibrous medium was modeled as a periodic array of circular cylinders, in a hexagonal arrangement, using the boundary element method. The area and volume average methods were applied to relate the pore scale to the representative elementary volume scale. The permeability of the modeled fibrous medium was calculated from the Darcy's law with the volume-averaged Darcy velocity. The slip coefficient, interfacial velocity, effective viscosity and shear jump coefficients at the interface were obtained with the averaged velocities at various permeabilities or Darcy numbers. Copyright © 2008 John Wiley & Sons, Ltd.

Received 6 August 2007; Revised 21 May 2008; Accepted 8 August 2008

KEY WORDS: cylinder array; fibrous porous medium; slip coefficient; effective viscosity; shear jump; interface condition

1. INTRODUCTION

Flow past a fibrous porous medium has interesting engineering applications, one of which is the swirling flow around porous scaffolds in bioreactors. To analyze flow with a porous medium, it is needed to couple the flow equations of the fluid and porous regions by using the interfacial boundary conditions. The interfacial conditions will also influence the heat and mass transfer across the interface.

To investigate the interfacial boundary conditions, simple models of flow through a channel partially filled with a porous medium have been considered. Most previous studies have been based

*Correspondence to: H. T. Low, Division of Bioengineering Engineering, National University of Singapore, 9 Engineering Drive 1, Singapore 117576, Singapore.
†E-mail: mpelowht@nus.edu.sg
‡Associate Professor.

on the representative elementary volume (REV) scale approach as modeling of a general porous pore scale structure is complex. However, for fibrous porous medium there were a few simplified models using a periodic array of cylinders. In such a flow model the permeability of the fibrous medium could be readily varied by the diameter of the cylinders or its spacing.

1.1. Permeability of porous medium

For the porous medium, an important parameter is permeability. Theoretical and numerical predictions of permeability have been made based on of approximations of the pore structure. Kozeny [1] approximated the porous medium by tortuous capillaries to develop an expression for the permeability. In the Carman–Kozeny model [2], a hydraulic diameter is defined from the specific surface area and porosity of the packed bed of particles. By applying the Poiseuille equation, the permeability is obtained in terms of the particle diameter, porosity and a Carman–Kozeny constant. The Carman–Kozeny model has been commonly used for granular porous media.

For fibrous media, due to its anisotropy, it is more appropriate to model them by arrays of cylinders. The permeability is obtained from the drag resistance across the cylinders. Two extreme cases were considered to obtain a closed-form solution for the whole range of porosity: closed packed and widely spaced cylinders.

The lubrication theory by Keller [3] is used for low porosities when the cylinders are closely packed. The pressure drop over the small gap between cylinders can be calculated analytically to give the permeability of the array [4]:

$$\frac{K}{d^2}=\frac{1}{12}\frac{(1-l_n^2)^2}{l_n^3}\left[3l_n\frac{\arctan\left[\sqrt{\dfrac{1+l_n}{1-l_n}}\right]}{\sqrt{1-l_n^2}}+\frac{1}{2}l_n^2+1\right]^{-1} \tag{1}$$

where d is the cylinder diameter, K is the permeability of the porous medium and l_n is the ratio of half the center spacing divided by the cylinder radius and can be expressed by the volume fraction as:

$$l_n^2=\frac{4}{\pi}v_f$$

The unit cell model is used for high porosities when the cylinders are widely spaced. It assumes that the cylinders are spaced far away so that the region can be divided into independent cells. Thus, the arrangement of the fibers has no effect on the solution. Typically, a circular cell is adopted with the cylinder located in the centre, whose radius depends on the porosity. From the drag on the cylinder the permeability can be obtained [4]:

$$\frac{K}{d^2}=-\frac{l_e^2}{16}\left[\ln(l_e)-\frac{3}{4}+l_e^{-2}-\frac{l_e^4}{4}\right] \tag{2}$$

where l_e is the ratio of the cylinder radius to the cell radius and is related to volume fraction of the porous medium by:

$$l_e^2=\frac{1}{v_f}$$

Different mathematical treatments have been used in the cell model based on the Stokes flow. For example, there are the free-surface models of Happel [5] with zero drag force and Kuwabara

DOI: 10.1002/fld

[6] with vorticity-free boundary condition. There are also methods using Fourier series to calculate the drag force of the cylinder in the cell model, for example those of Hasimoto [7] and Sangani and Acrivos [8, 9]. The method of singularities was used by Lord Rayleigh [10] and Drummond and Tahir [11]. Wang [12–14] used the eigenfunction expansion method.

In addition to methods for the extreme cases, there is a hybrid model of Bruschke and Advani [15], which attempts to predict the permeability over the full porosity range. The approach combines functions from both the lubrication and the cell models. Weighting functions, which depend on the porosity, are used to make the solution tend asymptotically to the extreme cases of lubrication or cell models. The asymptotic model gives a smooth transition from lubrication to cell model, which covers the middle range of porosity. The asymptotic model is given in terms of the porosity [15]

$$\frac{K}{d^2}=\frac{1}{16(1-\phi)}\left[\ln\left(\sqrt{\frac{1}{1-\phi}}\right)-\frac{3}{4}+(1-\phi)-\frac{(1-\phi)^2}{4}\right] \tag{3}$$

where ϕ is the porosity.

1.2. Interfacial flow for homogeneous porous media

In many applications involving porous media, they are bounded on one side by a flowing fluid layer. In most modeling, both fluid and porous media were assumed to be homogeneous. There are primarily two ways to deal with the interfacial boundary conditions. One is the slip boundary condition using slip coefficients [16, 17] and the other is no-slip boundary condition. Various flow models of the slip and no-slip interface boundary conditions are summarized in Table I.

Beavers and Joseph [16] proposed the slip boundary condition and presented some experimental results in which the channel size was varied, while keeping the pressure gradient constant. Their results showed that the slip coefficient increased with increasing porosity. However, experiments by Taylor [17] showed that for grooved plate, the slip coefficient increased with decreasing permeability, probably because a grooved plate was different from a porous medium.

For the no-slip boundary condition, the velocity is assumed continuous at the interface. The flow models can be classified into three major types according to the conditions of the velocity gradient and shear stress at the interface. The first type assumes continuity of both velocity gradient and shear stress [18, 19, 24]. The second type has non-continuity of velocity gradient but it assumes

Table I. Models of interface boundary conditions between a porous medium and a fluid layer.

Model	Velocity	Interface shear stress	References
1	$u_+\neq u_-$	$\left.\frac{\mathrm{d}u}{\mathrm{d}y}\right\|_{y=0^+}=\frac{\alpha}{\sqrt{K}}(u_{y=0}-u_D)$	[16, 17]
2	$u_+=u_-$	$\left.\frac{\mathrm{d}u}{\mathrm{d}y}\right\|_-=\left.\frac{\mathrm{d}u}{\mathrm{d}y}\right\|_+$	[18, 19]
3	$u_+=u_-$	$\mu_{\mathrm{eff}}\left.\frac{\mathrm{d}u}{\mathrm{d}y}\right\|_-=\mu\left.\frac{\mathrm{d}u}{\mathrm{d}y}\right\|_+$	[20]
4	$u_+=u_-$	$\frac{\mu}{\phi}\left.\frac{\mathrm{d}u}{\mathrm{d}y}\right\|_--\mu\left.\frac{\mathrm{d}u}{\mathrm{d}y}\right\|_+=\mu\frac{\beta_O}{\sqrt{K}}u_{y=0}$	[21, 22]
5	$u_+=u_-\mu$	$\left.\frac{\mathrm{d}u}{\mathrm{d}y}\right\|_--\mu\left.\frac{\mathrm{d}u}{\mathrm{d}y}\right\|_+=\mu\frac{\beta_C}{\sqrt{K}}u_{y=0}$	[23]

DOI: 10.1002/fld

continuity of shear stress, which is satisfied by using an effective viscosity for the porous medium region [20]. The third type has non-continuity of both velocity gradient and shear stress [21–23, 25].

The non-continuity of shear stress condition at the interface was developed by Ochoa-Tapia and Whitaker [21, 22] based on the non-local form of the volume averaging method. The function for the jump coefficient indicates dependence on permeability and porosity and was complex to solve. The coefficient was expected to be of order one, and may be either positive or negative. It was noted that the parameter depends on $\sqrt{K}/\delta$ where δ is the thickness of the boundary region.

Goyeau *et al.* [25] introduced a heterogeneous continuously varying transition layer between the homogeneous fluid and porous regions. The jump parameter was derived as an explicit function of the effective properties of the transition layer. The parameter is also related to the variations of the velocity in the transition layer, which is an unknown in the problem.

Recently, Chandesris and Jamet [23] presented a model in which the shear jump is built on fluid stress rather than effective stress. A single volume average transport equation in the whole domain was used. A heterogeneous continuously varying transition zone was introduced between the homogeneous fluid and porous regions. The flow problem inside the heterogeneous transition zone was solved using the method of matched asymptotic expansion. This solution enables the derivation of the interfacial boundary conditions to be applied in a flow model in which the homogeneous fluid and porous media are separated by a discontinuous interface. An explicit function for the stress jump coefficient was obtained, which only depends on the characteristics of the porous medium (porosity and permeability) in the transition zone. Subsequently, Chandesris and Jamet [26] proposed an explicit relation between the jump parameters, the location of the discontinuous interface, and the structure of the transition region. In a recent paper Valdes-Parada *et al.* [27] derived a stress jump boundary condition, using the volume averaging method, which is free of adjustable coefficients. The jump condition involves a mixed stress tensor which combines the global and Brinkman stresses at the interface region.

1.3. Interfacial flow for fibrous porous media

There were a few studies giving solutions which describe the interfacial flow for fibrous porous media. Most studies were modeled by flow in a channel partially filled with an array of cylinders. Usually the slip velocity and effective viscosity were investigated.

Larson and Higdon [28] analyzed the shear flow near the surface of a porous medium, as modeled by cylindrical array, using the boundary integral method. The slip velocity and dimensionless effective viscosity were presented as functions of solid-volume fraction. The slip coefficient was found to be sensitive to the definition of the interface, which they defined to be at the centre of the outermost cylinder.

Sahraoui and Kaviany [29] also modeled the porous medium by cylindrical arrays and used the finite difference method to study the interfacial boundary conditions. The slip coefficient was presented in terms of Reynolds number and the distribution of the local effective viscosity was given. Their results of slip coefficient agree well with the experiments of Beavers and Joseph [16].

James and Davis [30] used a singularity method to solve the flow field for cylindrical arrays of large porosity (greater than 0.9). Their calculations showed that the external flow penetrated the porous medium very little. The slip velocity was found to be about 0.4 of that predicted from the Brinkman model (based on effective viscosity).

There is no information on the stress jump coefficient. As described above, this condition of non-continuity of both velocity gradient and shear stress has been proposed in recent REV models

DOI: 10.1002/fld

of interfacial flow between fluid and porous media. However, the stress jump coefficient has not been compared with experiment or direct pore scale modeling.

1.4. Scope and objectives

One of the main objectives was to consider the boundary conditions at the interface between fluid layer and fibrous porous medium. The fibrous medium is modeled by an array of infinitely long circular cylinders and the aspect ratio is not varied. Different porosity is varied by changing the cylinder diameter. The slip coefficient, interfacial velocity, effective viscosity and stress jump coefficients are determined.

2. NUMERICAL MODEL

2.1. Mathematical formulation

The physical configuration and the coordinate systems are shown in Figure 1(a). The interface is at $y=0$, and the top and bottom walls are at $y=\pm H$. The porous medium is simulated as hexagonal arrays of infinitely long circular cylinders, which is bounded at the top by free fluid and at the bottom by a solid wall. The flow is transverse or perpendicular to the axis of cylinders. The periodic boundary condition is applied at the inlet and outlet of the channel. The channel flow is driven by a constant pressure gradient. The porosity was changed by changing the cylinder radius. The interface position was chosen to be the plane, which is tangent to the outer edges of cylinders in the first row [16, 29, 30].

The governing equation for the whole channel region is the steady Stokes equation:

$$\mu\nabla^2 u-\nabla p=0 \tag{4}$$

where μ is the fluid viscosity, u is the velocity and p is the pressure.

The boundary element method (BEM) is used to solve the Stokes equation. The cylinders are discretized into boundary elements of circular arcs. The boundary integral equations of two-dimensional Stokes flow for velocity are given below [31, 32]:

$$u_j(x_0)=u_j^{\infty}(x_0)-\frac{1}{4\pi\mu}\sum_{q=1}^{N_p}\int_{C_q} G_{ji}(x_0,x)\,f_i^{D}(x)\,\mathrm{d}l(x)$$

$$-\frac{1}{4\pi}\sum_{q=1}^{N_p}\int_{C_q} u_i^{\infty}(x,x_0)T_{ijk}(x,x_0)n_k(x)\,\mathrm{d}l(x) \tag{5}$$

where the subscript C_q is the contour of qth particle, N_p is the number of particles, n is the unit normal vector pointing into the fluid, f_i^D is the disturbance component of the hydrodynamic traction and G_{ji} is the unidirectional periodic Green's function for flow in a channel bounded by two parallel planes. The polar coordinate integral method is used to avoid the integral singularity.

2.2. Volume averaging method and dimensionless parameters

It is crucial to recognize that what is being solved is the local momentum transport problem. To relate the pore scale variations to the REV scale behavior, area and volume averages must be taken.

DOI: 10.1002/fld

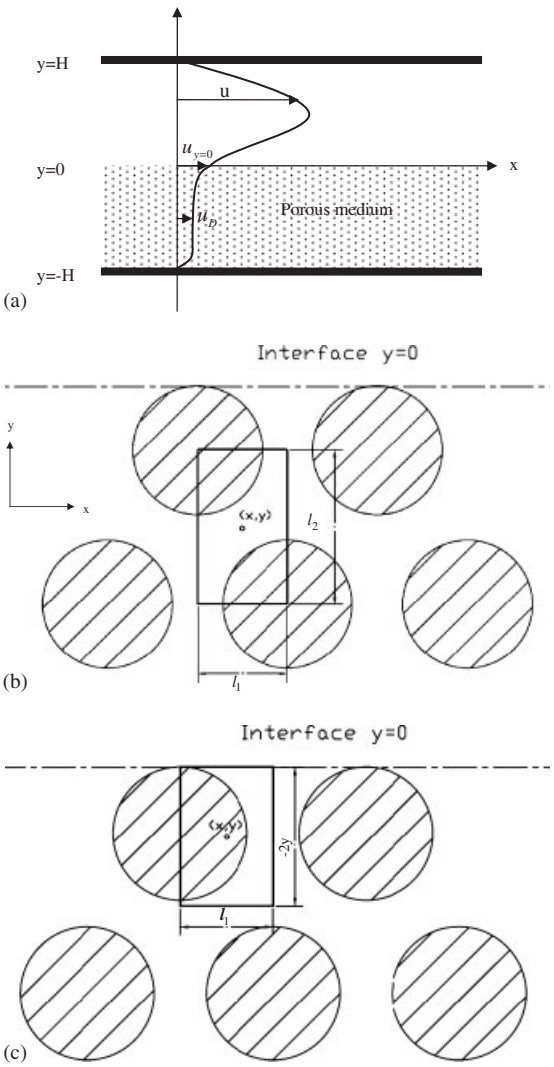

Figure 1. (a) Channel partially filled with fibrous porous medium; (b) a unit cell showing the representative elementary volume; and (c) an averaging volume near the interface.

For a channel flow partially filled with a porous medium modeled as an array of circular cylinders, the two-dimensional array is spatially periodic in the x direction. For this type of theoretical modeling, the averaging volume has been discussed in previous studies [28, 29, 33, 34].

For periodic array of cylinders, the length-scale constraint has been discussed by Whitaker [33] and Kaviany [34]. The volume average methods are valid when the following length-scale constraint is satisfied:

$$l_1 \cdot l_2 \ll L^2 \tag{6}$$

DOI: 10.1002/fld

where L is the channel characteristic length and l_1, l_2 are the cell dimensions. In the present study, the REV is shown in Figure 1(b), where the point (x, y) is at the cell center, l_1 is the cell dimension in x direction and l_2 is the cell dimension in y direction.

A justification of the present representative region is necessary to establish whether the length constraint is satisfied. In the present study there were 16 rows of cylinders in the y direction and $l_1 = l_2/\sqrt{3}$. Thus $l_1 \cdot l_2/H^2 \approx 1/15\sqrt{3} = 0.051$. To enforce the length constraint more rigorously, a larger number of rows of cylinders are needed, which would require larger computation resources. For comparison, James and Davies [30] used 5–20 rows of cylinders in their study.

The interfacial velocity is defined from its area average along the interface [29]:

$$\langle u \rangle_{A,y=0} \equiv \frac{1}{l_1} \int_0^{l_1} u(x, 0)\, \mathrm{d}x \tag{7}$$

where the bracket symbol $\langle\,\rangle_A$ represents area average. The volume average velocity is defined as [29]:

$$\langle u \rangle_V (y) \equiv \frac{1}{l_1 \cdot l_2} \int_{x-l_1/2}^{x+l_1/2} \int_{y-l_2/2}^{y+l_2/2} u(x, y)\, \mathrm{d}y\, \mathrm{d}x \tag{8}$$

where the bracket symbol $\langle\,\rangle_V$ represents volume average, which is independent of x as the array is periodic in the x direction.

To calculate the velocity gradients near the interface, the averaging volume must be carefully chosen so that the velocity variations near the interface can be reflected accurately. Furthermore, the averaging volume should ensure that the volume-averaged interfacial velocity is in agreement with that of the area-averaged values. Sahraoui and Kaviany [29] proposed that for any point y that is located between 0 and $-l_2/2$, the averaging volume is taken as $-2yl_1$ (see Figure 1(c); note y is negative), and the volume-averaged velocity is defined as:

$$\langle u \rangle_V (y) \equiv \frac{1}{-2yl_1} \int_{-2y}^{0} \int_{x-l_1/2}^{x+l_1/2} u(x, y')\, \mathrm{d}x\, \mathrm{d}y' \tag{9}$$

The permeability in the porous region is calculated using Darcy's law:

$$\frac{\mathrm{d}P}{\mathrm{d}x} = \frac{\mu}{K} u_\mathrm{D} \tag{10}$$

where $\mathrm{d}P/\mathrm{d}x$ is the pressure gradient, μ is the fluid dynamic viscosity and $u_\mathrm{D} = \langle u \rangle_V (y \to -\infty)$ is the Darcy velocity, which is a volume-averaged velocity over a local REV positioned deep into the porous medium. Noted that in the following parts, all the velocity u represents area- or volume-averaged velocities.

The velocity, distance and permeability are non-dimensionalized as [35]:

$$U = \frac{u}{u_\mathrm{D}} \tag{11a}$$

$$Y = \frac{y}{H} \tag{11b}$$

$$Da = \frac{K}{H^2} \tag{11c}$$

where H is the channel semi-width of flow region as shown in Figure 1(a). Da is Darcy number.

DOI: 10.1002/fld

3. RESULTS AND DISCUSSION

3.1. Permeability of fibrous porous medium

There have been analytical studies of unbounded flow through infinite and semi-infinite lattices of infinitely long cylinders [28, 29, 34, 36]. A numerical study on bounded flow has been given by James and Davies [30]. The present numerical results of permeability are compared with the previous studies.

Figure 2(a) and (b) shows the non-dimensional permeability K/d^2. It increases exponentially with increasing porosity, tending to infinitely a large value when the porosity is close to unity. A large porosity is associated with a small cylinder diameter d and a large permeability K, so that K/d^2 becomes large.

The cell, lubrication and asymptotic models are shown in Figure 2(a) for comparison with the present result. It is seen that the present results tend toward the cell model at high porosity and toward the lubrication model at low porosity. The present result is consistent with the assumptions of both models. The present result shows good agreement with the asymptotic model.

The results are compared with the Carman–Kozeny model in Figure 2(b), which has a Carman–Kozeny constant k. It is seen that with k from 0.2 to 17.9, the Carman–Kozeny model bounds the present numerical results. The present results may be approximately fitted by the Carman–Kozeny model with a constant $k=1.5$. However, note that the Carman–Kozeny constant varies with porosity, though not so obvious in the present results.

Figure 2(c) shows the permeability K/A as a function of solid volume fraction $c=1-\phi$ for hexagonal array of circular cylinders, where A is the area of the unit cell as defined by Larson and Higdon [28]. The comparison shows that the present results are in good agreement with those of Larson and Higdon [28]. The agreement is better at high solid fraction. Note that Larson and Higdon's [28] model is for infinite array, but the present array is bounded by free fluid at the top and solid wall at the bottom.

3.2. Volume-averaged velocity profiles

Figure 3(a) and (b) shows the velocity profile at two permeabilities. In Figure 3(a), different element numbers are used to check the convergence. It is seen that 64 elements per cylinder are sufficient. Also presented in Figure 3(b) is an enlarged figure of the domain used for calculations of the velocity gradient near the interface.

The velocities are non-dimensionalized by the average Darcy velocity u_{D}. Thus, the non-dimensional velocity in the porous medium is near to unity. At larger permeability, the Darcy velocity is larger, though not depicted by the non-dimensional plot. The maximum velocity in the fluid layer is much larger than that in the porous medium, well above an order of magnitude larger (see Figure 3(a) and (b)). In the REV scale results of Alazmi and Vafai [35] their maximum velocities are 130–1300 times of the Darcy velocity. However their Darcy numbers are smaller, from 10^{-3}–10^{-4} compared with the present 7.3×10^{-3}–10.1×10^{-3}. In the present velocity profiles (Figure 3(a) and (b)), the maximum velocity is greater at smaller permeability, which is consistent with the velocity results of Alazmi and Vafai [35]. It can be explained that, with constant pressure gradient, there is much more flow at the fluid side compared with that at the porous medium; the porous flow is lower at smaller permeability.

DOI: 10.1002/fld

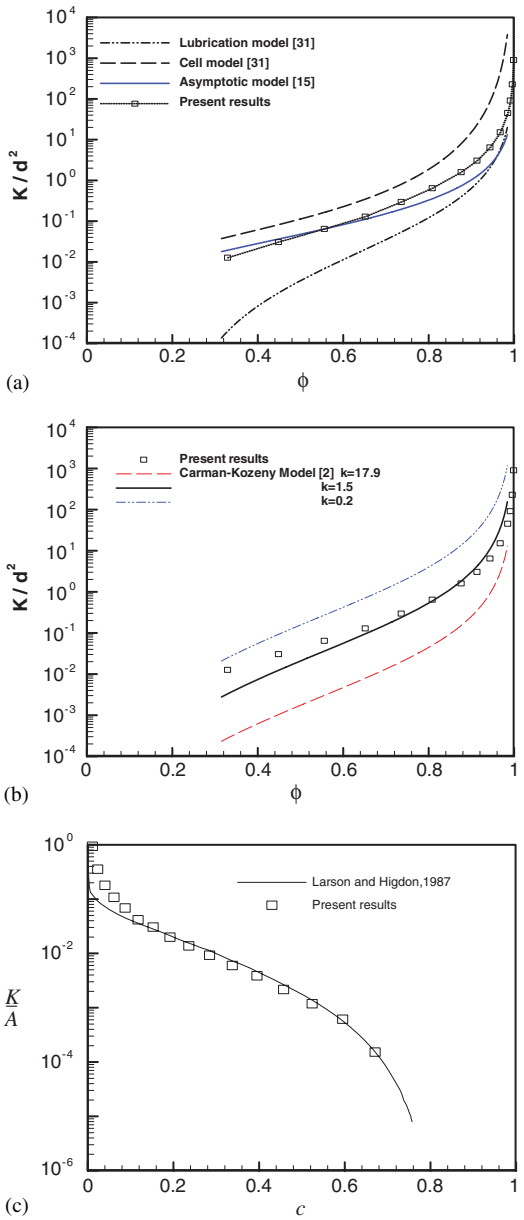

Figure 2. Permeability of porous media formed by cylinder arrays: (a) comparison with cell, lubrication and asymptotic models; (b) comparison with the Carman–Konzeny model; and (c) comparison with the Larson and Higdon study.

DOI: 10.1002/fld

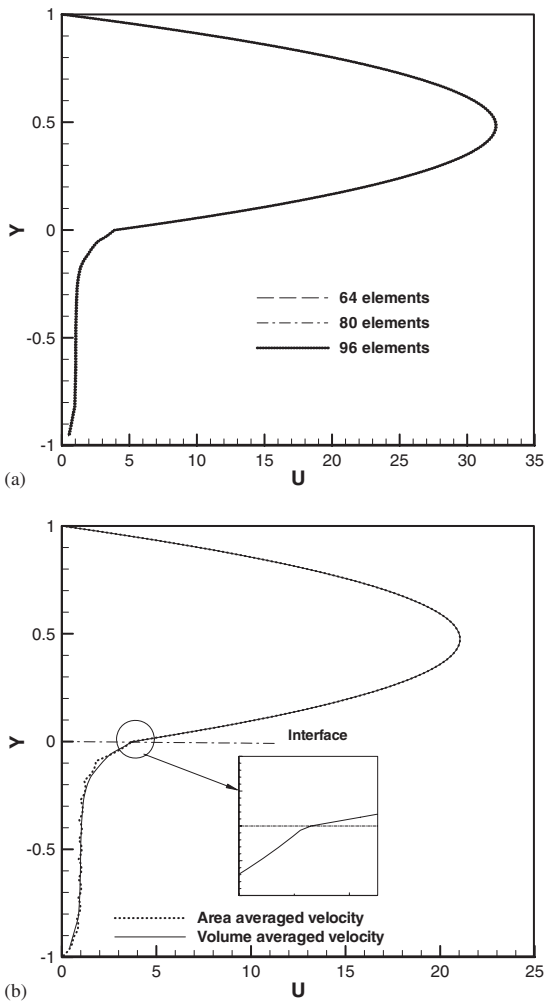

Figure 3. Non-dimensional averaged velocity profile: (a) convergence study at different element numbers; at $K = 2.93 \times 10^{-2}$ or $Da = 7.3 \times 10^{-3}$ and (b) an enlarged velocity profile at interface; at $K = 4.30 \times 10^{-2}$ or $Da = 10.1 \times 10^{-3}$.

3.3. Interfacial boundary conditions

3.3.1. Slip boundary condition. The slip boundary condition has been used in the homogeneous modeling of interface between fluid and porous media. The interfacial shear is related to the interface velocity $u_{y=0}$ at the interface by a slip coefficient α:

$$\left.\frac{\mathrm{d}u}{\mathrm{d}y}\right|_{y=0^+} = \frac{\alpha}{\sqrt{K}}(u_{y=0} - u_D) \tag{12a}$$

Using the slip boundary condition, together with the no-slip boundary condition at the impermeable wall, the velocity distribution in the fluid side may be found. The interfacial velocity and slip

DOI: 10.1002/fld

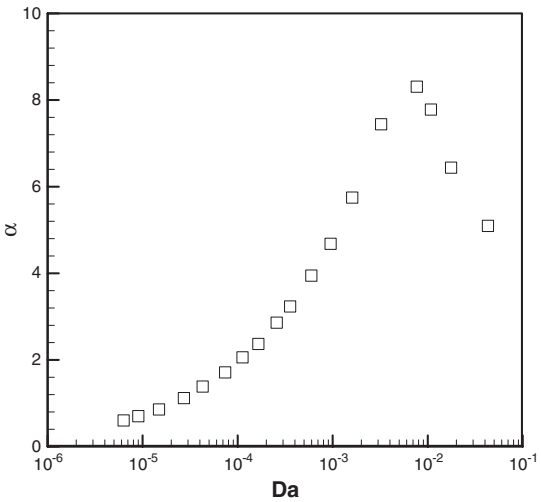

Figure 4. Slip coefficient versus Darcy number.

coefficient may be related by analysis:

$$\frac{u_{y=0}}{u_D} = \frac{1}{2}\frac{1+2\alpha\sqrt{Da}}{Da+\alpha\sqrt{Da}} \tag{12b}$$

Figure 4 shows the slip coefficient α (calculated using Equation (12a)) at various Darcy numbers. The slip coefficient varies between 0.4 and 8.4 and the average value is 5 over the present range of *Da*.

In Beavers and Joseph [16] experiments, the slip coefficient varies from 0.1 to 4, as permeability increases. It is difficult to make detailed comparison as Beavers and Joseph [16] specified pore size and not Darcy number. It is interesting that their experimental slip coefficients and the present results are of the same order even though the structures of the porous media were very different. A numerical study on array of cylinders has been carried out by Sahraoui and Kaviany [29], and the slip coefficient increases from 1.3 to 4.2 as porosity increases from 0.4 to 0.8. As compared with their numerical results, the present results are of the same order.

The interfacial velocity at the top of the fibrous medium is presented in Figure 5. Also presented is the prediction of interfacial velocity using Equation (12b), based on Darcy's law with the slip boundary condition. The slip coefficient (from Figure 4) was used. It is seen that, at large Darcy number 0.05, the interfacial velocity is around two times lesser when compared with the present results. The differences increase to around five times at low Darcy number 10^{-4}. In the analytical work of Vafai and Thiyagaraja [24], for Darcy number from 10^{-4} to 0.063, their interfacial velocity results agreed with the hypothesis proposed by Beavers and Joseph [16] that the fluid side velocity gradient at the interface is proportional to the slip velocity.

3.3.2. No shear jump boundary condition. In the no shear jump boundary condition, a shear term is added to the Darcy's law to account for velocity gradient at the interface. The velocity there

DOI: 10.1002/fld

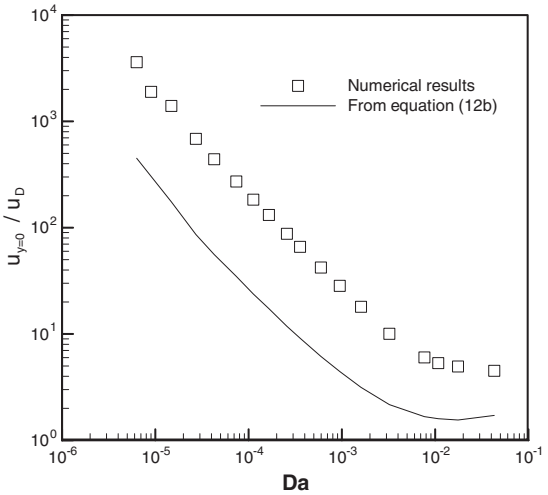

Figure 5. Dimensionless interface velocity versus Darcy number.

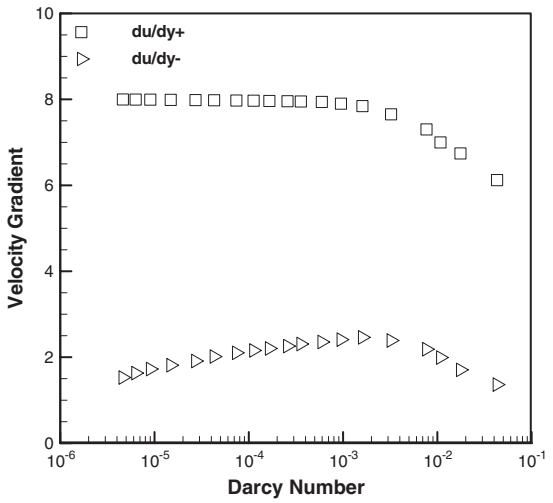

Figure 6. Velocity gradients at interface versus Darcy number.

is assumed continuous and so is the shear stress through the use of an effective viscosity μ_{eff}, assumed uniform in the porous medium, where

$$\mu_{\text{eff}} \left.\frac{\mathrm{d}u}{\mathrm{d}y}\right|_{-} = \mu \left.\frac{\mathrm{d}u}{\mathrm{d}y}\right|_{+} \tag{13}$$

The velocity gradients at the fluid and porous sides are shown in Figure 6; the gradients are non-continuous at the interface as expected. When Darcy number varies from 4×10^{-6} to 3×10^{-3}, the velocity gradient on the fluid side decreases very slightly, but that on the porous side increases

DOI: 10.1002/fld

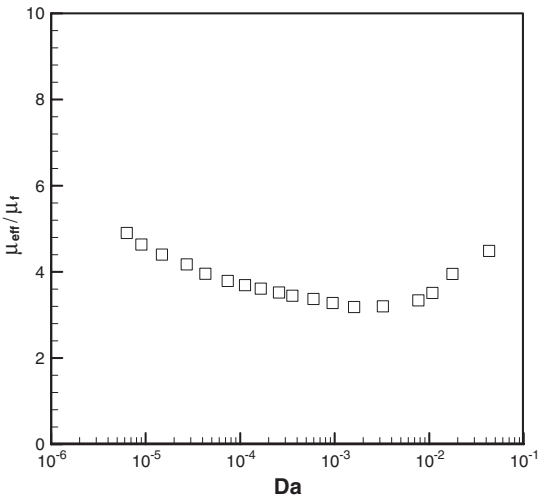

Figure 7. Dimensionless effective viscosity versus Darcy number.

slightly. When Darcy number is larger than 3×10^{-3}, both the fluid side and the porous side velocity gradients decrease significantly. From the ratio of velocity gradients at the fluid and porous media sides of the interface, the effective viscosity was found and presented in Figure 7 as a function of Darcy number. The dimensionless effective viscosity μ_{eff}/μ_f varies from around 3.1 to 5 for the present range of Darcy number.

In the experiments of Gilver and Altobelli [37], μ_{eff}/μ_f was found to be between 5 and 9 at low Reynolds number for large porosity $\phi = 0.972$. The present result is of the same order compared with the experiment results. However, note that the experimental result is for flow normal to a porous plug, which is different from the present parallel flow past the interface.

Sahraoui and Kaviany [29] have carried out numerical study on flow near the interface of a square array of cylinders and μ_{eff}/μ_f was estimated to vary from 0.7 to 2 when porosity increases from about 0.5 to 0.8. In the numerical study of shear flow past a hexagonal cylindrical array by Larson and Higdon [28], μ_{eff}/μ_f varies from 0.9 to 3 when porosity increases from 0.1 to 1.0. As compared with the previous numerical studies, the present dimensionless effective viscosity is of the same order.

3.3.3. Shear jump boundary condition. Like the above no shear jump boundary condition, the porous medium is modeled by the Darcy–Brinkman equation. The velocity at the interface is continuous. However, there is a shear stress jump at the interface given by:

$$\frac{\mu}{\phi}\frac{\mathrm{d}u}{\mathrm{d}y}\bigg|_{-} - \mu\frac{\mathrm{d}u}{\mathrm{d}y}\bigg|_{+} = \beta_0 \frac{\mu}{\sqrt{K}} u_{y=0} \tag{14a}$$

where β_0 is the shear jump coefficient.

The above stress jump boundary condition was derived by Ochoa-Tapia and Whitaker [21] based on the non-local form of the volume-averaged momentum equation. Note that this stress jump equation has an effective viscosity term μ/ϕ for the porous medium.

DOI: 10.1002/fld

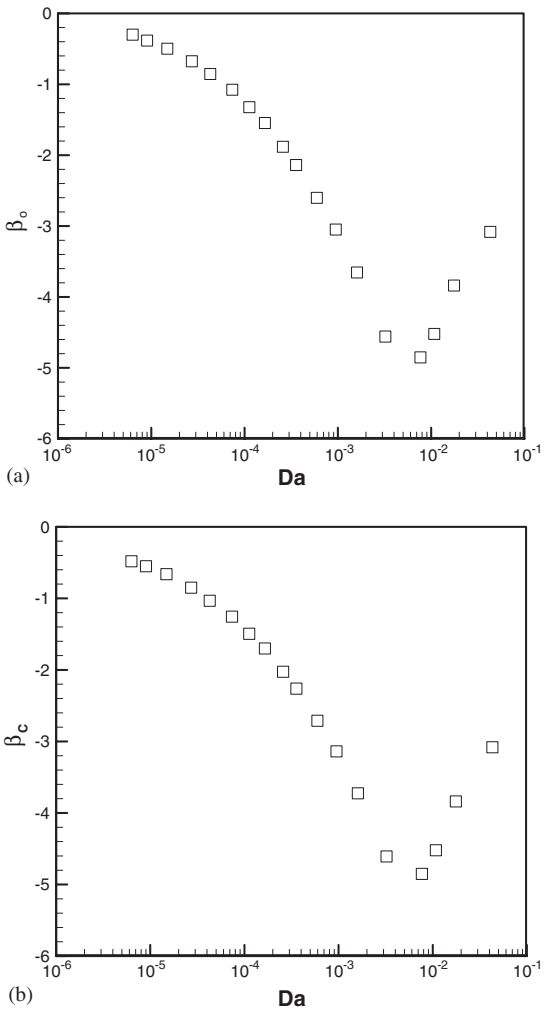

Figure 8. Shear jump coefficient versus Darcy number: (a) β_0 in Ochoa-Tapia and Whitaker's model and (b) β_C in Chandesris and Jamet's model.

The above equation is applied to the present numerical data of porosity, velocity gradients, permeability and interfacial velocity to determine the shear jump coefficient. The shear jump coefficient β_0 is presented in Figure 8(a) as a function of Darcy number. The shear jump coefficient is seen to vary from around 0 to -4.8 for the present range of Darcy numbers.

In the study of Ochoa-Tapia and Whitaker [22], β_0 was estimated to range from 1.5 to -1.0. This range of β_0 was obtained by adjusting it, so that their fractional excess flow rate due to porous medium showed a good fit with the experimental data of Beavers and Joseph [16]. The present results of β_0 are of the same order as Ochoa-Tapia and Whitaker [22]. However, it is difficult to make further comparison as their porosity was arbitrarily specified as 0.4. The porous media of Beavers and Joseph [16] are made of foam metal (lattice type) and aloxite (granular type) whose

DOI: 10.1002/fld

pore sizes ranged from 0.013 to 0.045 in. Though the present porous medium structure is very different from that of Beavers and Joseph [16], it is interesting that the shear jump coefficients are of the same order.

Another model of shear stress jump at the interface is that of Chandesris and Jamet [23], given by:

$$\mu \frac{\mathrm{d}u}{\mathrm{d}y}\bigg|_{-} - \mu \frac{\mathrm{d}u}{\mathrm{d}y}\bigg|_{+} = \beta_{\mathrm{C}} \frac{\mu}{\sqrt{K}} u_{y=0} \tag{14b}$$

where β_{C} is the shear jump coefficient. Note that this stress jump equation has fluid viscosity term μ for the porous medium unlike Equation (14a). The above equation was applied to the present numerical data of porosity, velocity gradients, permeability and interfacial velocity to determine the shear jump coefficient β_{C}.

The shear jump coefficient is presented in Figure 8(b). The jump coefficient varies from around -0.5 to -4.8 for the present range of Darcy numbers. In the study of Chandesris and Jamet [23], β_{C} was found to be between 4.28 and -0.637 in order to obtain good fit with Beavers and Joseph's [16] experimental data of the fractional increase in flow rate. The present coefficient shows similar trend as that of Chandesris and Jamet's [23] in which the coefficient decreases with increasing porosity. However, the present β_{C} is always of negative value, which is plausible if the velocity gradient of the porous side is always smaller than that of the fluid side.

4. CONCLUSIONS

A numerical study, using the BEM, was carried out on the flow through a channel partially filled with fibrous porous medium, which was modeled as a periodic, hexagonal array of cylinders. The flow is transverse to the cylinders and the interfacial boundary conditions were analyzed. The slip coefficient varies from around 0.4 to 8.4 for the present range of permeability. Using the slip coefficients, the slip boundary model gives an interfacial velocity, which is less than the present results by around 2–5 times. The effective viscosity varies from around 3.1 to 5 for the present permeability. The stress jump coefficient is of order one, which is consistent with previous literature. However, it is interesting that the present jump coefficients are negative in value. The present results may give some indication of the range of values of the coefficients that are needed as empirical inputs to the various models of interfacial boundary conditions. The interfacial conditions noted from the present pore scale modeling may be of interest to REV modeling of flow and heat transfer condition at the interface between fluid and porous media.

REFERENCES

1. Kozeny CF. Uber kapillare Leitung des Wassers im Boden. *Sitzungsberichte der Akademie der Wissenschaften* 1927; **136**:271–306.
2. Carman PC. Fluid flow through granular beds. *Transactions of the Institution of Chemical Engineers* 1937; **15**: 150–166.
3. Keller JB. Viscous flow through a grating or lattice of cylinders. *Journal of Fluid Mechanics* 1964; **18**(1):94–96.
4. Sadiq TAK, Advani SG, Parnas RS. Experimental investigation of transverse flow through aligned cylinders. *International Journal of Multiphase Flow* 1995; **21**:755–774.
5. Happel J. Viscous flow relative to arrays of cylinders. *AIChE Journal* 1959; **5**:174–177.

DOI: 10.1002/fld

6. Kuwabara S. The forces experienced by randomly distributed parallel circular cylinders or spheres in a viscous flow at small Reynolds numbers. *Journal of the Physical Society of Japan* 1959; **14**(4):527–532.
7. Hasimoto H. On the periodic fundamental solutions of the Stokes equations and their application to viscous flow past a cubic array of cylinders. *Journal of Fluid Mechanics* 1959; **5**(2):317–328.
8. Sangani AS, Acrivos A. Slow flow through a periodic array of spheres. *International Journal of Multiphase Flow* 1982; **8**(4):343–360.
9. Sangani AS, Acrivos A. A slow flow past periodic arrays of cylinders with application to heat transfer. *International Journal of Multiphase Flow* 1982; **8**(3):193–201.
10. Rayleigh L. On the influence of obstacles arranged in rectangular order upon the properties of a medium. *Philosophical Magazine* 1892; **34**:481–502.
11. Drummond JE, Tahir MI. Laminar viscous flow through regular arrays of parallel solid cylinders. *International Journal of Multiphase Flow* 1984; **10**(5):515–540.
12. Wang CY. Stokes flow through an array of rectangular fibers. *International Journal of Multiphase Flow* 1996; **22**(1):185–194.
13. Wang CY. Longitudinal flow past cylinders arranged in a triangular array. *Applied Mathematical Modeling* 1999; **23**(3):219–230.
14. Wang CY. Stokes flow through a rectangular array of circular cylinders. *Fluid Dynamics Research* 2001; **29**(2): 65–80.
15. Bruschke MV, Advani SG. Flow of generalized Newtonian fluids across a periodic array of cylinders. *Journal of Rheology* 1993; **37**(3):479–498.
16. Beavers GS, Joseph DD. Boundary conditions at a naturally permeable wall. *Journal of Fluid Mechanics* 1967; **30**:197–207.
17. Taylor GI. A model for the boundary condition of a porous material. Part 1. *Journal of Fluid Mechanics* 1971; **49**:319–326.
18. Vafai K, Kim SJ. Fluid mechanics of the interface region between a porous medium and a fluid layer—an exact solution. *International Journal of Heat and Fluid Flow* 1990; **11**:254–256.
19. Neale G, Nader W. Practical significance of Brinkman's extension of Darcy's law: coupled parallel flows within a channel and a bounding porous medium. *Canadian Journal of Chemical Engineering* 1974; **52**:475–478.
20. Kim SJ, Choi CY. Convective heat transfer in porous and overlying fluid layers heated from below. *International Journal of Heat and Mass Transfer* 1996; **39**:319–329.
21. Ochoa-Tapia JA, Whitaker S. Momentum transfer at the boundary between a porous medium and a homogeneous fluid I: theoretical development. *International Journal of Heat and Mass Transfer* 1995; **38**:2635–2646.
22. Ochoa-Tapia JA, Whitaker S. Momentum transfer at the boundary between a porous medium and a homogeneous fluid II: comparison with experiment. *International Journal of Heat and Mass Transfer* 1995; **38**:2647–2655.
23. Chandesris M, Jamet D. Boundary conditions at a planar fluid–porous interface for a Poiseuille flow. *International Journal of Heat and Mass Transfer* 2006; **49**(13–14):2137–2150.
24. Vafai K, Thiyagaraja R. Analysis of flow and heat transfer at the interface region of a porous medium. *International Journal of Heat and Mass Transfer* 1987; **30**:1391–1405.
25. Goyeau B, Lhuillier D, Gobin D, Velarde MG. Momentum transport at a fluid–porous interface. *International Journal of Heat and Mass Transfer* 2003; **46**:4071–4081.
26. Chandesris M, Jamet D. Boundary conditions at a fluid–porous interface: an a priori estimation of the stress jump coefficients. *International Journal of Heat and Mass Transfer* 2007; **50**:3422–3436.
27. Valdes-Parada FJ, Goyeau B, Ochoa-Tapia JA. Jump momentum boundary condition at a fluid–porous dividing surface: derivation of the closure problem. *Chemical Engineering Science* 2007; **62**:4025–4039.
28. Larson RE, Higdon JL. Microscopic flow near the surface of two-dimensional porous media. Part 2. Transverse flow. *Journal of Fluid Mechanics* 1987; **178**:119–136.
29. Sahraoui M, Kaviany M. Slip and no-slip velocity boundary conditions at interface of porous, plain media. *International Journal of Heat and Mass Transfer* 1992; **35**:927–943.
30. James DF, Davis AMJ. Flow at the interface of a model fibrous porous medium. *Journal of Fluid Mechanics* 2001; **426**:47–72.
31. Pozrikidis C. *Boundary Integral and Singularity Methods for Linearized Viscous Flow*. Cambridge University Press: Cambridge, 1992.
32. Pozrikidis C. *A Practical Guide to Boundary Element Methods with the Software Library BEMLIB*. Chapman & Hall/CRC: New York, 2002.
33. Whitaker S. *The Method of Volume Averaging*. Kluwer Academic Publishers: Dordrecht/Boston/London, 1999.

DOI: 10.1002/fld

34. Kaviany M. *Principles of Heat Transfer in Porous Media*. Springer: New York, 1991.
35. Alazmi B, Vafai K. Analysis of fluid flow and heat transfer interfacial conditions between a porous medium and a fluid layer. *International Journal of Heat and Mass Transfer* 2001; **44**:1735–1749.
36. Barrere J, Gipouloux O, Whitaker S. On the closure problem for Darcy's law. *Transport in Porous Media* 1992; **7**:209–222.
37. Gilver RC, Altobelli SA. A determination of the effective viscosity for the Brinkman–Forchheimer flow model. *Journal of Fluid Mechanics* 1994; **258**:355–370.

DOI: 10.1002/fld